Material Characterization Using Artificial Neural Network

S. Swaddiwudhipong [a], K.K. Tho [a], Z.S. Liu [b] and J. Hua [a]

[a] Department of Civil Engineering , National University of Singapore Singapore 119260

[b] Institute of High Performance Computing, 1 Science Park Road, #01-01, Singapore 117528

(cvesomsa@nus.edu.sg, g0202383@nus.edu.sg, liuzs@ihpc.a-star.edu.sg, cvehj@nus.edu.sg)

Summary

Indentation experiments have been carried out over the past century to determine hardness of materials. Modern indentation machines have the capability to continuously monitor load and displacement to high precision and accuracy. In recent years, research interests have focussed on methods to extract material properties from indentation load-displacement curves. Analytical methods to interpret the indentation load-displacement curves are difficult to formulate due to material and geometric nonlinearities as well as complex contact interactions. In the present study, an artificial neural network model was constructed for interpretation of indentation load-displacement curves. Large strain-large deformation finite element analyses were first carried out to simulate indentation experiments. The data from finite element analyses were then used to train the artificial neural network model. The artificial neural network model was able to accurately determine the material properties when presented with load-displacement curves which were not used in the training process. The proposed artificial neural network model is robust and directly relates the characteristics of the indentation load-displacement curve to the elasto-plastic material properties.

1 Introduction

Instrumented sharp indentation tests are widely carried out for mechanical characterization of materials. Traditionally, indentation tests are carried out to determine the hardness of the materials. Modern indentation machines have the capability to continuously monitor load and displacement to high precision and accuracy. Recent research efforts focus on the interpretation of indentation load-displacement curves to extract the other basic mechanical properties, such as Young's modulus, yield strength and strain-hardening exponent. Doerner and Nix (1986) and Oliver and Pharr (1992) pioneered methods to extract Young's modulus of materials from the unloading part of indentation load-displacement curves. Subsequently, Cheng and Cheng (1998, 1999) derived a set of dimensionless functions to relate the characteristics of the indentation load-displacement curve with the elasto-plastic properties of the material. Dao et al. (2001) proposed a new set of dimensionless functions and a forward and reverse analysis scheme based on extensive finite element simulations. Swaddiwudhipong et al. (2004) demonstrated that the load-displacement curves from dual indenters are essential for unique recovery of the three elasto-plastic material properties.

In the present study, an artificial neural network (ANN) model is constructed for material characterization based on dual sharp indenters. The numerical data from finite element analyses are used for training and verification of the ANN model. The proposed artificial neural network model is robust and accurately relates the characteristics of the indentation load-displacement curve to the elasto-plastic material properties.

2 Finite element simulation of indentation test

Large strain and large deformation axisymmetric finite element analyses were carried out using ABAQUS, a commercial finite element software. Conical indenters with half-angles of 60.0° and 70.3° are modelled as rigid bodies in the finite element models. As the effect of friction is negligible for any indenters with half-angle larger than 60° (Bucaille et al. 2003), frictionless contact is assumed in the present finite element model.

Materials obeying power law strain-hardening were considered in this study. For such materials, the uniaxial true stress-true strain relationship can be expressed as

$$\sigma = E\varepsilon \quad \text{for } \sigma \le Y \tag{1a}$$

$$\sigma = R\varepsilon^n \text{ for } \sigma \ge Y \tag{1b}$$

In Eq.(1), E is the Young's modulus, Y the yield stress, R the strength coefficient and n the strain-hardening exponent. Enforcing continuity at $\sigma = Y$ gives

$$R = Y\left(\frac{E}{Y}\right)^n \tag{2}$$

The elasticity effect of the indenter can be considered in the analysis through the replacement of the actual Young's modulus, E of the targeted materials by a reduced Young's modulus, expressed in Eq.(3) (Giannakopoulos and Suresh 1999; Dao et al. 2001; Chollacoop et al. 2003).

$$E^* = \left[\frac{1-\nu^2}{E} + \frac{1-\nu_i^2}{E_i}\right]^{-1} \tag{3}$$

In Eq.(3), E^* is the reduced Young's modulus, E_i and ν_i are the Young's modulus and Poisson's ratio of the indenter respectively. A constant Poisson's ratio of 0.33 is used throughout this study.

3 Fundamental aspects of load-displacement curves

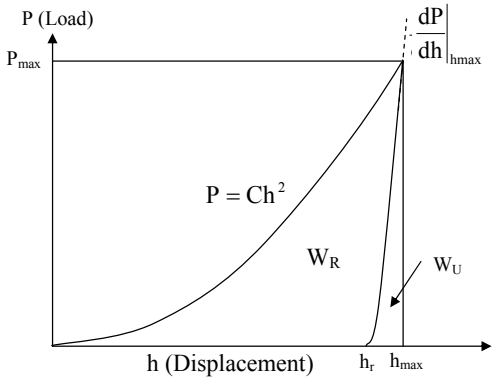

Figure 1: Schematic representation of a typical load-displacement curve

A typical load-displacement curve in an indentation experiment is shown in Fig.(1).

3.1 Loading curve

The loading part of an instrumented sharp indentation generally follows Kick's Law which can be expressed as

$$P = Ch^2 \tag{4}$$

where P is the indentation load, h the penetration depth measured from the surface and C a constant curvature.

Based on cavity expansion analogy, the following relationship between C and the three material parameters (E^*, Y, n) can be established.

$$\frac{C}{Y} = f_{1,\theta}\left(\frac{E^*}{Y}, n\right) \tag{5}$$

where θ is the half-angle of the indenter.

Eq. (5) is consistent with the relationship derived by Cheng and Cheng (1998) using dimensional analysis.

3.2 Relationship between indentation work and total work done

Cheng and Cheng (1998) derived the following dimensionless function.

$$\frac{W_T - W_U}{W_T} = \prod_{\omega}\left(\frac{Y}{E}, \nu, \theta\right) \tag{6}$$

where W_T is the area under the loading curve and W_U the area under the unloading curve.

Denoting ($W_T - W_U$) by W_R and for a particular value of Poisson's ratio and half-angle of the indenter, Eq. (6) becomes

$$\frac{W_R}{W_T} = f_{2,\theta}\left(\frac{E^*}{Y}, n\right) \tag{7}$$

4 Artificial Neural Network Model

4.1 Model Definition

For θ = 60.0° and 70.3°, Eqs. (5) and (7) yield respectively

$$\left.\frac{C}{Y}\right|_{60.0°} = f_{1,60.0°}\left(\frac{E^*}{Y}, n\right) \tag{8}$$

$$\left.\frac{C}{Y}\right|_{70.3°} = f_{1,70.3°}\left(\frac{E^*}{Y}, n\right) \tag{9}$$

$$\left.\frac{W_R}{W_T}\right|_{60.0^\circ} = f_{2,60.0^\circ}\left(\frac{E^*}{Y}, n\right) \tag{10}$$

$$\left.\frac{W_R}{W_T}\right|_{70.3^\circ} = f_{2,70.3^\circ}\left(\frac{E^*}{Y}, n\right) \tag{11}$$

Dividing Eq.(8) by Eq.(9) leads to Eq.(12).

$$\frac{C_{60.0^\circ}}{C_{70.3^\circ}} = \frac{f_{1,60.0^\circ}\left(\frac{E^*}{Y}, n\right)}{f_{1,70.3^\circ}\left(\frac{E^*}{Y}, n\right)} = f_3\left(\frac{E^*}{Y}, n\right) \tag{12}$$

It has been shown earlier (Swaddiwudhipong et al. 2004, Tho et al. 2004) that the reverse analysis based on dual sharp indenters lead to unique solution of E^*/Y and n. Therefore, there exists a one-to-one mapping of $(C_{60.0^\circ})/(C_{70.3^\circ})$, $(W_R/W_T)_{60.0^\circ}$ and $(W_R/W_T)_{70.3^\circ}$ to E^*/Y and n. Two artificial neural networks, denoted as ANN-1 and ANN-2, are constructed for the reverse analysis of instrumented indentation results. ANN-1 is constructed to map $(C_{60.0^\circ})/(C_{70.3^\circ})$, $(W_R/W_T)_{60.0^\circ}$ and $(W_R/W_T)_{70.3^\circ}$ to E^*/Y and n while the mapping of E^*/Y and n to $(C_{60.0^\circ}/Y)$ and $(C_{70.3^\circ}/Y)$ is handled by ANN-2. The solution procedure is summarized in the flowchart shown in Fig.(2). From the indentation load-displacement curves of both indenters, the quantities $C_{60.0^\circ}$, $C_{70.3^\circ}$, $(W_R/W_T)_{60.0^\circ}$ and $(W_R/W_T)_{70.3^\circ}$ can be evaluated. By providing the values of these quantities into ANN-1, the ratio of E^*/Y and n can be established. The results are then substituted into ANN-2 to determine $(C_{60.0^\circ}/Y)$ and $(C_{70.3^\circ}/Y)$. Once $C_{60.0^\circ}$ and $C_{70.3^\circ}$ are known, Y can be calculated from either $(C_{60.0^\circ}/Y)$ or $(C_{70.3^\circ}/Y)$. Consequently, E^* can be evaluated from the ratio of E^*/Y established earlier. The actual value of Young's modulus, E, can then be obtained from Eq.(3).

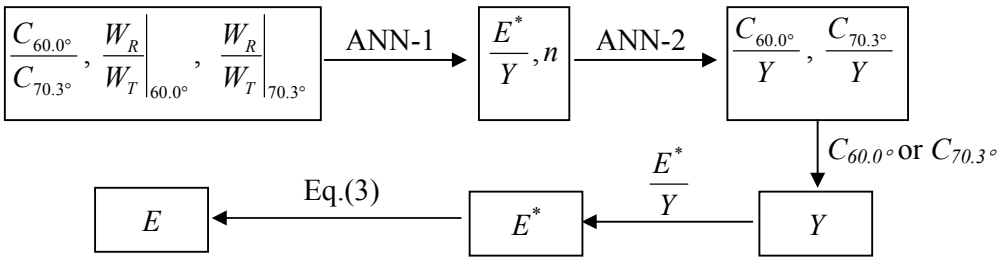

Figure 2: Flowchart illustrating the solution procedure

4.2 Model Construction

Back-propagation multilayer feedforward ANNs (ANN-1 and ANN-2) were created using the Neural Network Toolbox in Matlab 6.5 package. Both ANN-1 and ANN-2 comprise the input layer, a hidden layer and the output layer. The number of neurons in the input and output layers of the ANNs are identical to the number of input and output parameters respectively while the number of neurons in the hidden layer of the neural network is calibrated during the training and

validation process.The tangent sigmoid transfer function is used in the hidden layer while the linear transfer function is assigned to the output layer.

4.3 Training and Validation

The ANNs are trained by introducing a set of examples of proper network behaviour to the ANNs. During training, the learning rule is used to iteratively adjust the weights and biases of the network in order to move the network outputs closer to the target values by minimizing the network performance indicator. The Levenberg-Marquardt training algorithm, which has a higher rate of convergence, is used for the training of both ANN-1 and ANN-2.

The data for training and validation of ANN-1 and ANN-2 were obtained numerically through 500 large strain, large deformation finite element analyses encompassing a domain of E^*/Y from 10 to 1000 and n varying from 0.0 to 0.6 for each of the conical indenters. Out of the 500 sets of input and output data, 400 sets were randomly assigned as training data while the remaining 100 sets were used for validation purpose. The mean square error, MSE, of the network outputs and the target values is used as the network performance indicator. The characteristics of ANN-1 and ANN-2 are summarised in Table 1.

Table 1: Characteristics of ANN-1 and ANN-2

	Range of outputs	Number of neurons in the hidden layer	Mean Square Error	
			Training	Validation
ANN-1	0 – 1	30	1.398E-05	4.609E-05
ANN-2	10-610	24	4.555E-02	5.215E-02

5 Results and Discussion

Finite element analyses were carried out to simulate indentation experiments on Al6061 and iron. The typical elasto-plastic material properties of these materials are used as inputs to the finite element model. The finite element results are summarised in Table 2. It should be noted that these sets of finite element results were not used in the training and validation process described in Section 4.3.

Table 2: Summary of finite element results for Al6061 and iron

Material	Conical indenter with half-angle of 60.0 degree		Conical indenter with half-angle of 70.3 degree	
	$C_{60.0^\circ}$ (GPa)	$C_{70.3^\circ}$ (GPa)	$(W_R/W_T)_{60.0^\circ}$	$(W_R/W_T)_{70.3^\circ}$
Al6061	10.740	27.200	0.952	0.921
Iron	24.598	55.513	0.949	0.925

The material properties predicted by the artificial neural network model are shown in Table 3 together with the actual material properties. It can be observed from Table 3 that the proposed artificial neural network model predicted the elasto-plastic material properties reasonably accurately.

Table 3: Prediction from artificial neural network model

	Al6061	Iron
E^* (GPa)		
Actual	72.363	170.789
Predicted	72.700	169.963

E (GPa)		
Actual	69.000	180.000
Predicted	69.343	178.971
Y (MPa)		
Actual	275.000	300.000
Predicted	276.320	297.880
n		
Actual	0.050	0.250
Predicted	0.049	0.253

6 Conclusion

The use of artificial neural networks enable the direct mapping of the characteristics of the indentation load-displacement curve to the elasto-plastic material properties. The proposed artificial neural network model can accurately predict the elasto-plastic properties of the material based on the indentation load-displacement curves of two conical indenters with different half-angles.

7 References

Bucaille, J.L., Stauss, S., Felder, E., Michler. 2003. Determination of plastic properties of metals by instrumented indentation using different sharp indenters. Acta Materialia 51:1663-1678.

Cheng, Y.T., Cheng, C.M., 1998. Scaling approach to conical indentation in elastic-plastic solids with work hardening. Journal of Applied Physics 84:1284-1291.

Cheng, Y.T., Cheng, C.M. 1999. Scaling relationships in conical indentation of elastic-perfectly plastic solids. International Journal of Solids and Structures 36:1231-1243.

Chollacoop, N., Dao, M., Suresh, S. 2003. Depth-sensing instrumented indentation with dual sharp indenters. Acta Materialia 51:3713-3729.

Dao, M., Chollacoop, N., Van Vliet. K.J., Venkatesh, T.A., Suresh, S. 2001. Computational modelling of the forward and reverse problems in instrumented sharp indentation. Acta Materialia 49:3899-3918.

Doerner, M.F., Nix, W.D. 1986. A method for interpreting the data from depth-sensing indentation instruments. Journal of Material Research 1:601-609.

Giannakopoulos, A.E., Suresh, S. 1999. Determination of elastoplastic properties by instrumented sharp indentation. Scripta Materialia 40:1191-1198.

Oliver, W.C., Pharr, GM. 1992. An improved technique for determining hardness and elastic modulus using load and displacement sensing indentation experiments. Journal of Material Research 7:1564-1583.

Swaddiwudhipong, S., Tho, K.K., S., Liu, Z.S., Zeng, K. 2004. Material characterization based on dual indenters. (submitted for publication).

Tho, K.K., Swaddiwudhipong, S., Liu, Z.S., Zeng, K. 2004. Uniqueness of reverse analysis from conical indentation tests. (submitted for publication).